Sensors and Materials, Vol. 26, No. 5 (2014) 291–298
MYU Tokyo

S & M 0993

Optical Fiber Relative Humidity Sensor Based on Fabry-Perot Interferometer Coated with Sodium-p-styrenesulfonate/Allyamine Hydrochloride Films

Qingmei Sui, Mingshun Jiang*, Zhongwei Jin,
Faye Zhang, Yuqiang Cao and Lei Jia

School of Control Science and Engineering, Shandong University, Jinan 250061, China

(Received December 24, 2013; accepted March 6, 2014)

Key words: optical fiber RH sensor, Fabry-Perot interferometer, electrostatic self-assembly, nanocoating, temperature insensitive

We report on a fiber optic relative humidity (RH) sensor by coating negatively charged poly(sodium-p-styrenesulfonate) (PSS) nanoparticles and positively charged poly(allyamine hydrochloride) (PAH) nanoparticles on the endface of an intrinsic Fabry-Perot interferometer (IFPI) by a layer-by-layer (LbL) electrostatic self-assembly method. The IFPI, formed by a section of a hollow-core photonic crystal fiber (HCPCF) and standard single-mode fibers (SMFs), is fabricated using a fusion splicer. The LbL electrostatic self-assembly process of a PAH/PSS multilayer is traced with a quartz crystal microbalance and shows a fast thickness growth. The optical response of the modified RH sensor to different RH values is evaluated on the basis of the maximum fringe contrast of the interference fringes in the reflective spectra. A high sensitivity of 0.08 dB/%RH is achieved. It shows response times of 2 and 6 s in the RH increasing and decreasing processes, respectively. In addition, the IFPI sensor has good stability and highly reversible performance. The proposed sensor shows excellent thermal stability as well.

1. Introduction

Optical-fiber-based relative humidity (RH) sensors have attracted increasing interest in recent years because of their distinct advantages such as immunity to electromagnetic noise, small size, anticorrosion property, high sensitivity, and remote sensing.[1–3] Related techniques include direct spectroscopic methods,[4] evanescent waves,[5–7] in-fiber grating,[6–12] and interferometric methods.[13] A variety of chemical reagents have been used as sensing elements to prepare optical fiber humidity sensors, such as cobalt

*Corresponding author: e-mail: sdujiangmingshun@163.com

chloride ($CoCl_2$),[14] cobalt oxide (Co_3O_4),[15] or crystal violet.[16] In most optical sensors, the sensitive reagents are immobilized in a solid matrix and attached to the fiber. The matrix serves to encapsulate the reagent such that it is accessible to the analyte while being impervious to leaching effects. A variety of polymers are being used in optical sensors, including silicones, poly (vinylchloride) (PVC), poly (tetrafluoroethylene) (PTFE), agarose, and cellulose derivatives.[17,18] The choice of the support matrix is governed by parameters such as mechanical stability, permeability to the analyte, and suitability for reagent immobilisation.[19] On the other hand, it may affect the performance of the sensor, particularly its selectivity and response time.

In our previous work, the use of poly (diallyldim-ethylammonium chloride)/poly (styrenesulfonate sodium salt) (PDDA/PSS)-coated Fabry-Perot (F-P) sensors[20] and TiO_2-nanoparticle-coated F-P sensors[21] had been investigated for refractive index measurement. The results indicated that the refractive index sensitivity of the coated F-P sensors could be effectively improved after the deposition of nanoparticle thin films.

In this paper, we present a humidity sensor consisting of an F-P interferometer modified by PAH/PSS films. In comparison with the other sensors, the sensor presented here has advantages of high sensitivity, large measurement range, and rapid response. The sensing mechanism is based on F-P tip Fresnel reflection interaction with the coating of the nanocomposites. As the incident light guided propagates through the sensing region, the reflected coefficients are affected by the change in the environmental parameter, i.e., humidity. This results in a modulated output from the fiber, which is used as the criterion for detecting the RH in the surrounding environment.

2. Theory of Principle

The optical fiber intrinsic Fabry-Perot interferometer (IFPI), formed by a section of a hollow-core photonic crystal fiber (HCPCF) and standard single-mode fibers (SMFs), is fabricated using a fusion splicer. Then, the film is coated on the tip of the F-P sensor endface by the LbL technique. The schematic of the coated F-P is shown in Fig. 1.

The schematic diagram of the thin-film-coated F-P sensor is shown in Fig. 1, which contains a short section of a hollow-core fiber. Three cavities, the hollow-core fiber cavity, SMF cavity, and film cavity, which contain four reflection surfaces (M1–M4), are formed. The lengths of the hollow-core fiber cavity, SMF cavity, and film cavity are L_1, L_2, and L_3, respectively. The cavity lengths of L_1 and L_2 are constants. The refractive

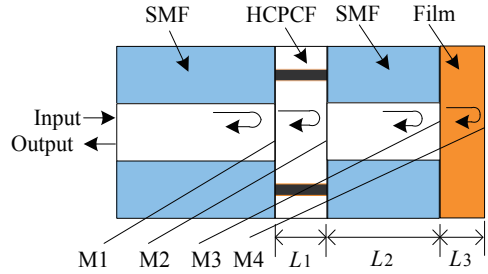

Fig. 1. (Color online) Schematic of coated F-P sensor.

indices of the SMF, HCPCF, film, and environment are denoted as n_0, n_h, n_f, and n_e, respectively. The power reflection coefficients at surfaces 1, 2, 3, and 4 are R_1, R_2, R_3, and R_4, respectively. The hollow-core photonic crystal fiber guides light by photonic band-gap effects, which is created via a delicate two-dimensional periodic lattice of glass webs and hollow channels.[22] Its refractive index can be regarded as $n_h = 1$. Thus, the power reflection coefficients R_1 and R_2 at the mirrors 1 and 2 are both equal to

$$R_1 = R_2 = (n_h - n_0)^2/(n_h + n_0)^2, \tag{1}$$

while the reflection coefficients R_3 and R_4 depending on the film refractive index and environment index can be expressed as

$$R_3 = (n_h - n_f)^2/(n_h + n_f)^2,\ R_4 = (n_f - n_e)^2/(n_f + n_e)^2. \tag{2}$$

The total reflected field from the sensor is given approximately by the sum of the first-order reflected fields from the four surfaces.[23–25] The total reflected electric field E_r can thus be given as

$$\begin{aligned} E_r = {} & \sqrt{R_1}E_i + (1 - A_1)(1 - R_1)\sqrt{R_2}E_i e^{-j2\beta L_1 + j\pi} \\ & + (1 - A_1)(1 - R_1)\cdot(1 - A_2)(1 - R_2)\sqrt{R_3}E_i e^{-j2\beta(L_1 + L_2)} \\ & + (1 - A_1)(1 - R_1)\cdot(1 - A_2)(1 - R_2)\cdot(1 - A_3)(1 - R_3)\sqrt{R_4}E_i e^{-j2\beta(L_1 + L_2 + L_3)}, \end{aligned} \tag{3}$$

where E_i is the input field, and A_1, A_2, and A_3 are the transmission loss factors at reflection surfaces 1, 2, and 3, respectively. β is the propagation constant of the guided mode of the fiber.

$$I_{total} = |E_r/E_i|^2 \tag{4}$$

The effects are practically the same for the four surfaces and mainly cause a change in the background light intensity. There is a π-phase shift at reflection surface 2, since light is reflected from an optically denser medium.

According to eqs. (3) and (4), variations in the refractive index of the coated film and the external medium will lead to changes in the reflectance at the fiber-film interface and, therefore, in the sensor output signal. Changes in the film thickness will also lead to changes in the reflectance at the fiber-film and film-external-medium interfaces.

When the coated F-P sensor is used in humidity detection, the generation of a signal can be analyzed in terms of two conceptual steps. The first one depends on the interactions that take place between the coated film and the external environment. In the second step, the humidity modifies the refractive index of the film, and hence, the transmitted light power. The stronger the interaction or modification of the refractive index of the film, the higher the sensitivity. Increasing the concentration of water vapor inside the chamber will result in the adsorption of water on the film surface. As a result, the overall refractive index of the film with adsorbed water will be lower than that of the degassed film. Therefore, increasing the water vapor concentration will result in decreasing reflectance.

In addition, the RH measurement based on eq. (4) is independent of the power of the input light. Since both the thermal expansion coefficient and thermooptic coefficient of the fiber are very small, the measurement should be insensitive to the temperature variation. No temperature compensation is therefore needed for the designed sensor.

3. Sensor Design

3.1 *Material*

Concentrated H_2SO_4, ethanol, poly(allyamine hydrochloride) (PAH) (*Mw* = 70000 g/mol), poly(sodium-p-styrenesulfonate) (PSS) (*Mw* = 70000 g/mol), and H_2O_2 were purchased from Aldrich. The deionized water used in all the experiments was purified in a three-stage Milli-Q Plus 185 purification system and had an initial resistivity that was greater than 18.2 MΩ cm.

3.2 *Fabrication of nanocoating*

In the process of sandwiched F-P sensor design, the lengths of the HCPCF and the subsequent SMF were chosen as 30 and 600 μm, respectively. The optical fiber F-P sensor tip was cleaned using a piranha solution (7:3 of concentrated H_2SO_4 and 30% H_2O_2), washed with large amounts of deionized water and dried with nitrogen, obtaining negatively charged substrates. The negatively charged tip was dipped into the positively charged PAH and negatively charged PSS solutions alternatively, each for 10 min at room temperature. Between polycation and polyanion immersions, the sensor endface was rinsed with deionized water three times (1 min each time) to remove the excess absorbed material and dried with nitrogen. The coating made by two dipping procedures was called a bilayer. The same cycle was repeated until the desired numbers of bilayers were deposited. The thickness of the nanocoating is characterized using a quartz crystal microbalance. The electrostatic self-assembly deposition of PAH/PSS and the relationship between film thickness and bilayer number are shown in Figs. 2(a) and 2(b),

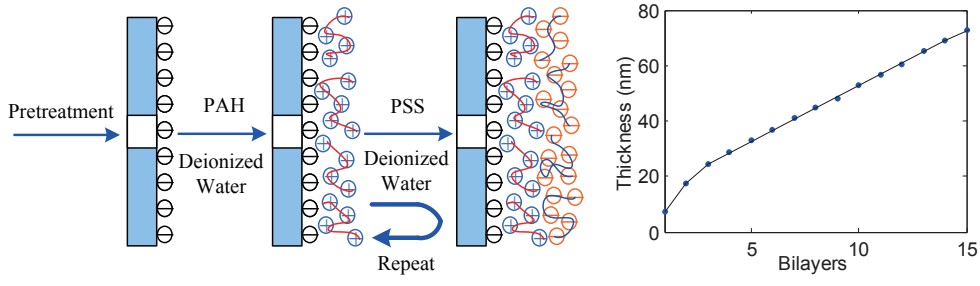

Fig. 2. (Color online) (a) Electrostatic self-assembly deposition of PAH/PSS. (b) Thickness growth of multilayers with increasing bilayer number.

respectively. We can see from Fig. 2(b) that the film thickness increases linearly with the bilayer number. The average thickness is 4 nm/bilayer.

The reflected spectra of the uncoated F-P sensor and F-P sensor coated with 15 layers are shown in Figs. 3(a) and 3(b), respectively. To achieve the highest measurement resolution, we should always use the fringe that has the maximum fringe contrast. To locate this particular fringe, we first locate the dip of the fringe envelope from the reflective spectrum, as shown Fig. 3(a) within the dip of the fringe envelope, and then identify the fringe that gives the maximum fringe contrast, which can be achieved by locating the absolute minimum dip (point B) and the adjacent peak (point A). The corresponding fringe contrast is given by $V = 10\log_{10}(R(\lambda_A)/R(\lambda_B))$. For the coated F-P sensor, the absolute minimum dip and the adjacent peak are B′ and A′, respectively. It can be seen that the fringe contrasts of spectra decreased at a certain degree (from 19.08 to 13.61 dB, with the 35% RH of the measurement environment). It mainly depends on the reflected light of the reflected surface M3 and reflected surface M4. It confirms the successful fabrication of the LbL electrostatic self-assembly nanocoating on the optical fiber F-P sensor.

4. Experiments and Analysis

This coated F-P sensor was then fixed in a specially designed plexiglass humidity chamber as shown in Fig. 4.

The chamber had provisions for passing the compressed air and moist air. A commercial moisture sensor based on capacitance phenomenon (from Rotronix, model: HygroFlex2) was fixed in the chamber for calibration. The ratio of compressed air to moist air that passed inside the chamber was controlled to change the humidity inside the chamber to different levels. The coated F-P sensor tip is firmly fixed in the chamber. A reflective optical analyzer instrument (MOI SM130) was utilized to measure the reflective spectrum of the F-P sensor. All data were real-time monitored using a

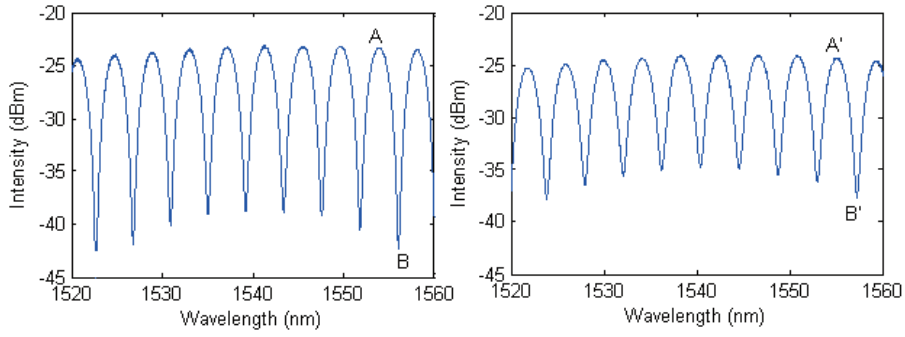

Fig. 3. (Color online) Interference spectra of F-P sensor before (a) and after (b) deposition of PAH/PSS multilayers.

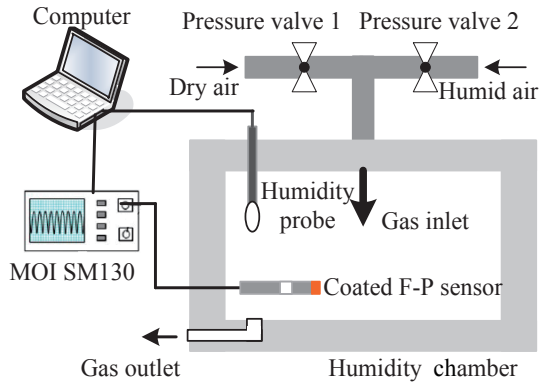

Fig. 4. (Color online) Experimental setup for measurement of relative humidity.

computer. The film-coated optical fiber F-P sensor with (PAH/PSS) 15 nanocoated layers was tested in a humidity chamber with different relative humidities ranging from 5 to 90%. Figure 5 shows the fringe contrast change of the coated sensor to different relative humidities. The RH detection sensitivity of 0.08 dB/%RH is obtained. As the intensity resolution of the MOI SM130 is 0.01 dB, an RH resolution of about 0.125% is achieved. It can also be seen that the fringe contrast of the coated RH sensor changes only slightly at the same RH environment during the 10-min measurement. The good stability performance is verified.

In addition, the time response of the coated sensor is tested from high RH to low RH and the reverse process. The optical spectrum analyzer keeps sweeping with a frequency of 1 kHz. As shown in Fig. 6, the same fringe contrasts of the coated sensor were maintained while it was set in the same RH, no matter what tested order (RH increasing or decreasing).

It can also be seen that when the RH rises, the response time (rise time: increasing from start to 90% of the measurement value) is 2 s, while in the RH decreasing process, its response time (fall time: decreasing from start to 90% of the measurement value) is 6 s, which is longer. It is because the water can quickly diffuse into the nanocoating. The response time can be further shorted by preparing a nanoporous multilayer film or a thinner multilayer film at the cost of decreasing sensitivity.

The thermal stability test measurement was carried out under a fixed humidity of 40% RH and changing the temperature from 20 to 100 °C. Figure 7 gives the experimental results. The fringe contrast was almost not affected (fluctuation <0.01 dB) by the temperature changes. These experimental results show that the proposed humidity sensor is temperature insensitive.

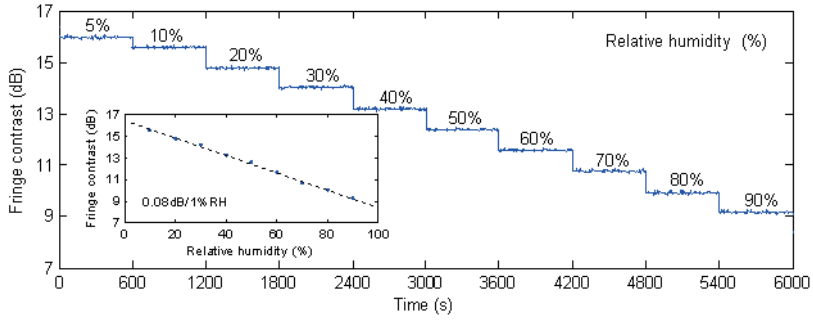

Fig. 5. (Color online) Relationship between humidity and fringe contrast.

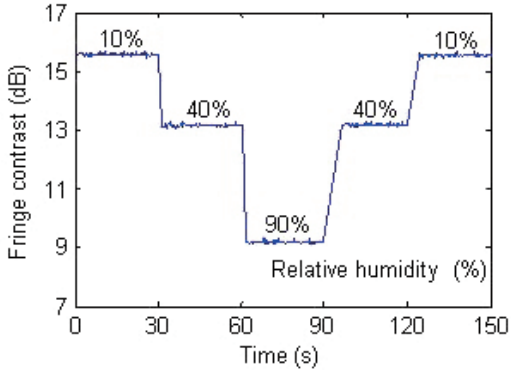

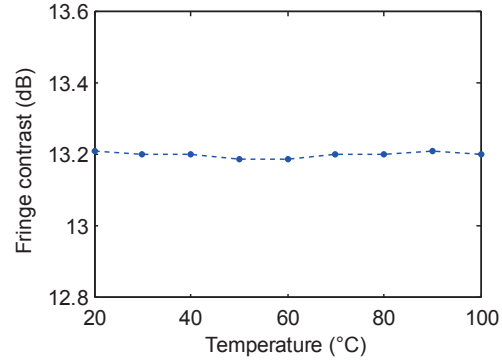

Fig. 6 (left). (Color online) Time response and repeatability.
Fig. 7 (right). (Color online) Thermal stability of proposed sensor.

5. Conclusions

PAH nanoparticles and PSS polyelectrolytes have been successfully fabricated for the first time on a sandwiched-structure F-P interferometer tip by the LbL electrostatic self-assembly technique to form a novel RH sensor. Experimental results show that the measurement range of 5–90% has been achieved with a maximum sensitivity of 0.08 dB/%RH. The response time is 2 s in the RH increasing process, whereas in the RH decreasing process, its response time is longer (6 s); moreover, the RH measurement is insensitive to temperature. It is expected that this sensor will be used in a wide range of applications, including meteorological services and in the chemical and food processing industries.

Acknowledgements

The authors gratefully acknowledge financial support for this work from the Natural Science Foundation of China (Grant No. 61074163) and the Natural Science Foundation of Shandong Province, China (Grant No. ZR2011FQ025).

References

1 J. Estella, P. de Vicente, J. C. Echeverria and J. J. Garrido: Sens. Actuators, B **149** (2010) 122.
2 B. D. Gupta and Ratnanjali: Sens. Actuators, B **80** (2001) 132.
3 Z. Zhao and Y. Duan: Sens. Actuators, B **160** (2011) 1340.
4 J. M. Corres, F. J. Arregui and I. R. Matias: Sens. Actuators, B **122** (2007) 442.
5 S. Q. Tao, C. B. Winstead, R. Jindal and J. P. Singh: IEEE Sens. J. **4** (2004) 322.
6 W. C. Wong, C. C. Chan, L. H. Chen, T. Li, K. X. Lee and K. C. Leong: Sens. Actuators, B **174** (2012) 563.
7 C. R. Zamarreno, M. Hernaez, P. Sanchez, I. Del Villar, I. R. Matias and F. J. Arregui: Procedia Eng. **25** (2011) 1385.
8 T. L. Yeo, T. Sun, K. T. V. Grattan, D. Parry, R. Lade and B. D. Powell: IEEE Sens. J. **5** (2005) 1082.
9 C. Chen, Y. Yu, R. Yang, C. Wang, J. Guo, Y. Xue, Q. Chen and H. Sun: J. Lightwave Technol. **31** (2013) 455.
10 L. Alwis, T. Sun amd K. T. V. Grattan: Sens. Actuators, B **178** (2013) 694.
11 S. Zhang, X. Dong, T. Li, C. C. Chan and P. P. Shum: Opt. Commun. **303** (2013) 42.
12 L. Alwis, T. Sun and K. V. Grattan: IEEE Sens. J.**13** (2013) 767.
13 A. Vijayan, M. Fuke, R. Hawaldar, M. Kulkarni, D. Amalnerkar and R. C. Aiyer: Sens. Actuators, B **129** (2008) 106.
14 S. K. Khijwania, K. L. Srinivasan and J. P. Singh: Sens. Actuators, B **104** (2005) 217.
15 M. Ando, T. Kobayashi and M. Haruta: Sens. Actuators, B **32** (1996) 157.
16 T. E. Brook, M. N. Taib and R. Narayanaswamy: Sens. Actuators, B **39** (1997) 272.
17 T. E. Brook and R. Narayanaswamy: Sens. Actuators, B **51** (1998) 77.
18 C. McDonagh, C. S. Burke and B. D. MacCraith: Chem. Rev. **108** (2008) 400.
19 P. C. A. Jeronimo, A. N. Araujo and M. Montenegro: Talanta **72** (2007) 13.
20 M. Jiang, Q. Li, J. Wang, W. Yao, W. Dong, Z. Jin, Q. Sui, J. Shi, F. Zhang and L. Jia: J. Lightwave Technol. 2013 (in press).
21 M. Jiang, Q. Li, J. Wang, Z. Jin, Q. Sui, Y. Ma, J. Shi, F. Zhang, L. Jia, W. Yao and W. Dong: Opt. Express **21** (2013) 3083.
22 Y. Zhao, R. Lv, Y. Ying and Q. Wang: Opt. Laser Technol. **44** (2012) 899.
23 Y. Rao, M. Deng, D. Duan and T. Zhu: Sens. Actuators, A **148** (2008) 33.
24 Z. L. Ran, Y. J. Rao, W. J. Liu, X. Liao and K. S. Chiang: Opt. Express **16** (2008) 2252.
25 C. Lee, C. Huang, C. Li and Y. You: Opt. Commun. **285** (2012) 439.